Magic wavelengths for optical cooling and trapping of potassium

M. S. Safronova,[1,2] U. I. Safronova,[3,4] and Charles W. Clark[2]

[1]*Department of Physics and Astronomy, 217 Sharp Lab, University of Delaware, Newark, Delaware 19716, USA*

[2]*Joint Quantum Institute, National Institute of Standards and Technology and the University of Maryland, Gaithersburg, Maryland 20899, USA*

[3]*Physics Department, University of Nevada, Reno, Nevada 89557, USA*

[4]*Department of Physics, University of Notre Dame, Notre Dame, Indiana 46556, USA*

We carry out a systematic study of the static and dynamic polarizabilities of the potassium atom using a first-principles high-precision relativistic all-order method in which all single, double, and partial triple excitations of the Dirac-Fock wave functions are included to all orders of perturbation theory. Recommended values and uncertainties are provided for the relevant electric-dipole matrix elements. Polarizabilities of the $4s$, $4p_j$, $5s$, $5p_j$, and $3d_j$ states are compared with other theoretical and experimental values when possible. We identify magic wavelengths for the $4s$-np transitions for $n = 4,5$, i.e., those wavelengths for which the two levels have the same ac Stark shifts. The magic wavelengths for the $4s$-$5p$ transitions are of particular interest for attaining a quantum gas of potassium at high phase-space density. We find 20 such wavelengths in the technically interesting region of 1050–1130 nm.

I. INTRODUCTION

Due to their applications in ultraprecise atomic clocks, degenerate quantum gases and quantum information, the magic wavelengths of atoms have become a subject of great interest in both experiments [1–4] and theory [5–15]. The energy levels of atoms trapped in a light field are shifted by an amount that is proportional to their frequency-dependent polarizability, so the difference in the energies of any two levels depends upon the trapping field. This difference is often called the "ac Stark shift."

The idea of a "magic" wavelength, λ_{magic}, at which there is no relative shift of a given pair of energy levels, was first proposed in Refs. [16,17] in the context of optical atomic clocks. An atom confined in a trap constructed of light with a magic wavelength for the clock transition will, to lowest order, have the same transition energy as it does in free space.

This idea has a number of other applications. A problem arises in cooling and trapping schemes, where the ac Stark shift of the cooling or trapping transition may lead to heating. Recent experiments in ^{6}Li [18] and ^{40}K [2] degenerate quantum gases in optical traps demonstrated temperature reductions by a factor of about 5 and phase-space density increases by at least a factor of 10 by laser cooling using ultraviolet (UV) transitions ($2s$-$3p$ and $4s$-$5p$, respectively) compared to conventional cooling with the visible or infrared D_1 and D_2 transitions. However, the ac Stark shifts due to trap light must be nearly the same for both levels in the transition to allow for efficient and uniform cooling [18]. This is accomplished by building the optical trap using light with the magic wavelength for the corresponding UV transitions. The use of the magic wavelengths is also advantageous for trapping and controlling atoms in high-Q cavities in the strong-coupling regime, so as to minimize decoherence in quantum computation and communication protocols [19], and in the implementation of the Rydberg gate for quantum computing with neutral atoms [20,21].

Variations on the magic wavelength idea include the use of multiple light fields to attain ac Stark shift cancellation [22] or to maximize differential response between different atomic species—for example, the "tune-out" wavelengths that trap one species but not another [23–25]. Design and evaluation of all these applications requires accurate data on atomic frequency-dependent polarizabilities. One goal of our present work is to provide a list of all magic wavelengths for potassium UV $4s$-$5p_j$ transitions in regions that are convenient for laser cooling of ultracold gases to high phase-space densities, as has been demonstrated in 2011 by McKay *et al.* [2].

In this paper we provide a list of magic wavelengths for the $4s$-$4p$ and $4s$-$5p$ transitions, calculate dc and ac polarizabilities for several low-lying states, and provide recommended values for a number of relevant electric-dipole transitions which are of interest to applications such as those described above. Where possible, we compare our results with available experimental [26] and high-precision theoretical values [27–30].

In Sec. II we summarize the calculation of electric-dipole matrix elements and static and dynamic polarizabilities as well as the estimation of their uncertainties. Some of the calculations reported here required evaluation of the electric-dipole matrix elements for very highly excited states, such as $14s$. These states are needed since the ac polarizabilities for the magic wavelengths of particular experimental interest (around 1050 nm) are dominated by the $5p$-nl transitions with $n = 12$–14. Such states were previously beyond the capabilities of the all-order method used here due to the large spatial extent of the orbitals. In this work, we resolved the numerical problems associated with such calculations and successfully demonstrated the stability of our approach. Our results are presented in Sec. III.

II. MATRIX ELEMENTS AND POLARIZABILITIES

The magic wavelengths for a specific transition are located by calculating the frequency-dependent polarizabilities of the

lower and upper states and finding their crossing points. The present approach to the calculation of atomic polarizabilities was discussed in Refs. [14,24,27,34–37], and we provide only a brief summary of the methods here. Unless stated otherwise, all specific data refers to the K atom, and we use the conventional system of atomic units, a.u., in which e, m_e, $4\pi\epsilon_0$, and the reduced Planck constant $\hbar$ have the numerical value 1. Polarizability in a.u. has the dimension of volume, and its numerical values presented here are expressed in units of a_0^3, where $a_0 \approx 0.052\,918$ nm is the Bohr radius. The atomic units for α can be converted to SI units via α/h [Hz/(V/m)^2] $=$ $2.488\,32 \times 10^{-8}\alpha$ (a.u.), where the conversion coefficient is $4\pi\epsilon_0 a_0^3/h$ and the Planck constant h is factored out.

We represent the polarizability $\alpha(\omega)$ of the K atom as the sum of the polarizabilities of the K$^+$ core and the valence polarizability, described by the sum over valence states [Eq. (1)]. The effect of the valence electron on the ionic K$^+$ core polarizability α_{core} is accounted for by the core-valence α_{vc} term. This term subtracts out the excitations from the ionic K$^+$ core to the occupied valence shell forbidden by the Pauli principle. Such approach is very well established and has been tested for a large number of atoms and ions, including systems with one, two, and three valence electrons. Particularly high-accuracy benchmarks were established for Na-like [38] and Mg-like ions [39], where very high-precision (0.1%) measurements of polarizabilities exist. We verified that the ionic core polarizability and α_{vc} term depend weakly on ω for the frequencies treated here and are approximated by their dc values calculated in the random-phase approximation (RPA) [40]. The contribution of the core polarizability (5.5 a.u.) is very small (1.9% of the static ground state static polarizability); $\alpha_{vc} = -0.18$ a.u. for the ground state and is smaller for the other states.

The valence contribution to frequency-dependent scalar α_0 and tensor α_2 polarizabilities is evaluated as the sum over intermediate k states allowed by the electric-dipole transition rules [40]

$$\alpha_0^v(\omega) = \frac{2}{3(2j_v + 1)} \sum_k \frac{\langle k\|d\|v\rangle^2 (E_k - E_v)}{(E_k - E_v)^2 - \omega^2},$$

$$\alpha_2^v(\omega) = -4C \sum_k (-1)^{j_v + j_k + 1} \begin{Bmatrix} j_v & 1 & j_k \\ 1 & j_v & 2 \end{Bmatrix}$$

$$\times \frac{\langle k\|d\|v\rangle^2 (E_k - E_v)}{(E_k - E_v)^2 - \omega^2},$$

(1)

where C is given by

$$C = \left(\frac{5j_v(2j_v - 1)}{6(j_v + 1)(2j_v + 1)(2j_v + 3)} \right)^{1/2}$$

and $\langle k\|d\|v\rangle$ are the reduced electric-dipole matrix elements. In these equations, ω is assumed to be at least several linewidths off resonance with the corresponding transitions. Linear polarization is assumed in all calculations.

We use the linearized version of the coupled cluster approach (also referred to as the all-order method), which sums infinite sets of many-body perturbation theory terms, for all significant terms in the equations above. The $4s$-np, $4p$-nl, $5s$-nl, and $3d$-nl transitions with $n \leqslant 26$ and $5p$-nl transitions with $n \leqslant 40$ are calculated using this approach [35,37].

As we noted in the Introduction, the present calculation required evaluation of the electric-dipole matrix elements for highly excited states, since the frequency-dependent polarizabilities for the $4s$-$5p$ magic wavelengths of particular experimental interest are dominated by the $5p$-nl transitions with $n = 12$–14. The difficulty with the application of the all-order method for these states results from the use of a complete set of Dirac-Fock (DF) wave functions on a nonlinear grid generated using B splines constrained to a spherical cavity. A large cavity with a radius of $R = 220a_0$ is needed to accommodate all valence orbitals with $ns = 4s$-$10s$, $np = 4p$-$10p$, and $nd = 3d$-$9d$. A cavity radius of $400a_0$ was chosen to accommodate additional valence orbitals with $ns = 11s$-$14s$, $np = 11p$-$13p$, and $nd = 10d$-$12d$. Our basis set consists of 70 splines of order 11 for each value of the relativistic angular quantum number κ for $R = 220a_0$ and 100 splines of order 13 for $R = 400a_0$. We have conducted test comparisons of the basis set energies with the actual DF values to demonstrate the numerical stability of this calculation. We note that calculations of the few highest $4s$-$4p$ magic wavelengths (above 680 nm) do not require such large basis sets, as the contributions of the highly excited states are not resonant for these wavelengths. We use available experimental energies for the $ns = 4s$-$11s$, $np = 4p$-$10p$, and $nd = 3d$-$12d$ states from [41] and theoretical all-order energies for other states with $n \leqslant 26$ ($n \leqslant 40$ for in the $4s$-$5p$ magic wavelength calculations). The remaining small contributions with $n > 26$ are calculated in the DF approximation. For example, the contributions from states with $n > 26$ give only 0.075 a.u. to the polarizability of the $4p_{1/2}$ state. We note that states with $n > 19$ in our basis have positive energies and provide a discrete representation of the continuum.

The evaluation of the uncertainty of the matrix elements in this approach was described in detail in [35,36]. Four all-order calculations were carried out, including two *ab initio* all-order calculations with and without the inclusion of the partial triple excitations and two other calculations that incorporated semiempirical estimates of high-order correlation corrections starting from both *ab initio* runs. The spread of these four values for each transition defines the estimated uncertainty in the final results when considered justified based on the dominant correlation contributions to the $E1$ matrix elements [35,36]. We note that this procedure does not work in the small number of cases where we cannot estimate uncertainty in the dominant contributions using the procedure described above. No uncertainties are listed for such matrix elements; however, their contributions are small, leading to negligible effects on the final uncertainties of the polarizabilities.

The absolute values of the reduced electric-dipole matrix elements used in our subsequent calculations and their uncertainties are listed in a.u. in Table I. We list only the most important subset of the several hundred matrix elements that were calculated in this work. The results are compared with recent coupled-cluster calculations including single, double, and perturbative triple excitations [CCSD(T)] of Ref. [28] and relativistic configuration interaction plus core polarization (RCICP) calculations of Ref. [29]. The present values are in excellent agreement with most of the CCSD(T) values of Ref. [28] with the exception of some $4p$-nd and $5p$-nd transitions. In these cases, the correlation corrections, and

TABLE I. Absolute values of the reduced electric-dipole matrix elements in K and their uncertainties in a.u. The present all-order values are given unless noted otherwise. The uncertainties are estimated where possible (see text).

Transition	Present	Other		Transition	Present	Other		Transition	Present	Other	
$4s$-$4p_{1/2}$	4.106(4)[a]	4.13(2)	[28]	$4s$-$4p_{3/2}$	5.807(7)[a]	5.84(2)	[28]	$4p_{3/2}$-$3d_{5/2}$	10.734(47)[b]	10.75(5)	[28]
		4.103	[29]			5.802	[29]			10.719	[29]
$4s$-$5p_{1/2}$	0.276	0.282(6)	[28]	$4s$-$5p_{3/2}$	0.406	0.416(6)	[28]	$4p_{3/2}$-$4d_{5/2}$	0.117(15)	0.260(5)	[28]
		0.263	[29]			0.389	[29]			0.155	[29]
$4s$ -$6p_{1/2}$	0.086	0.087(5)	[28]	$4s$-$6p_{3/2}$	0.130	0.132(6)	[28]	$4p_{3/2}$-$5d_{5/2}$	0.467(6)	0.374(5)	[28]
		0.076	[29]			0.116	[29]	$4p_{3/2}$-$6d_{5/2}$	0.471(7)	0.404(5)	[28]
$4s$-$7p_{1/2}$	0.039	0.041(5)	[28]	$4s$-$7p_{3/2}$	0.061	0.064(5)	[28]	$4p_{3/2}$-$7d_{5/2}$	0.409(7)	0.356(5)	[28]
$4s$-$8p_{1/2}$	0.023	0.023(3)	[28]	$4s$-$8p_{3/2}$	0.036	0.038(3)	[28]	$4p_{3/2}$-$8d_{5/2}$	0.349(5)	0.286(5)	[28]
$4s$-$9p_{1/2}$	0.015	0.016(3)	[28]	$4s$-$9p_{3/2}$	0.024	0.027(3)	[28]	$4p_{3/2}$-$9d_{5/2}$	0.299(4)		
$4s$-$10p_{1/2}$	0.011			$4s$-$10p_{3/2}$	0.018			$5p_{3/2}$-$3d_{5/2}$	9.57(10)	9.73(15)	[28]
$4p_{1/2}$-$6s$	0.903(4)	0.909(10)	[28]	$4p_{3/2}$-$6s$	1.279(5)	1.287(10)	[28]			9.574	[29]
$4p_{1/2}$-$7s$	0.476(2)	0.479(5)	[28]	$4p_{3/2}$-$7s$	0.673(3)	0.677(6)	[28]	$5p_{3/2}$-$4d_{5/2}$	22.93(8)	22.84(30)	[28]
$4p_{1/2}$-$8s$	0.314(2)	0.316(5)	[28]	$4p_{3/2}$-$8s$	0.444(2)	0.447(5)	[28]			22.93	[29]
$4p_{1/2}$-$9s$	0.230(1)	0.225(3)	[28]	$4p_{3/2}$-$9s$	0.325(2)	0.317(5)	[28]	$5p_{3/2}$-$5d_{5/2}$	1.19(4)	1.461(5)	[28]
$4p_{1/2}$-$10s$	0.1791(9)	0.171(3)	[28]	$4p_{3/2}$-$10s$	0.253(1)	0.242(5)	[28]	$5p_{3/2}$-$6d_{5/2}$	0.119(17)	0.045(5)	[28]
$4p_{1/2}$-$11s$	0.1452(8)			$4p_{3/2}$-$11s$	0.205(1)			$5p_{3/2}$-$7d_{5/2}$	0.318(15)		
$4p_{1/2}$-$3d_{3/2}$	7.979(35)[b]	7.988(40)	[28]	$4p_{3/2}$-$3d_{3/2}$	3.578(16)[b]	3.583(20)	[28]	$5p_{3/2}$-$8d_{5/2}$	0.335(12)		
		7.966	[29]			3.573	[29]	$5p_{3/2}$-$9d_{5/2}$	0.312(9)		
$4p_{1/2}$-$4d_{3/2}$	0.112(14)	0.220(5)	[28]	$4p_{3/2}$-$4d_{3/2}$	0.040(6)	0.088(5)	[28]	$3d_{3/2}$-$6p_{1/2}$	1.03(1)	1.04(1)	[28]
		0.140	[29]			0.053	[29]	$3d_{3/2}$-$7p_{1/2}$	0.497(5)	0.500(6)	[28]
$4p_{1/2}$-$5d_{3/2}$	0.333(5)	0.264(5)	[28]	$4p_{3/2}$-$5d_{3/2}$	0.155(2)	0.124(5)	[28]	$3d_{3/2}$-$8p_{1/2}$	0.317(3)	0.321(5)	[28]
$4p_{1/2}$-$6d_{3/2}$	0.341(5)	0.293(5)	[28]	$4p_{3/2}$-$6d_{3/2}$	0.157(2)	0.135(5)	[28]	$3d_{3/2}$-$9p_{1/2}$	0.228(3)	0.250(4)	[28]
$4p_{1/2}$-$7d_{3/2}$	0.298(5)	0.261(4)	[28]	$4p_{3/2}$-$7d_{3/2}$	0.136(2)	0.119(3)	[28]	$3d_{3/2}$-$10p_{1/2}$	0.176(2)		
$4p_{1/2}$-$8d_{3/2}$	0.254(4)	0.221(4)	[28]	$4p_{3/2}$-$8d_{3/2}$	0.116(2)	0.101(3)	[28]	$3d_{3/2}$-$6p_{3/2}$	0.464(5)	0.467(3)	[28]
$4p_{1/2}$-$9d_{3/2}$	0.218(3)			$4p_{3/2}$-$9d_{3/2}$	0.100(2)			$3d_{3/2}$-$7p_{3/2}$	0.224(2)	0.225(5)	[28]
$5s$-$4p_{1/2}$	3.885(8)	3.876(10)	[28]	$5s$-$4p_{3/2}$	5.54(1)	5.52(2)	[28]	$3d_{3/2}$-$8p_{3/2}$	0.143(1)	0.144(4)	[28]
		3.888	[29]			5.538	[29]	$3d_{3/2}$-$9p_{3/2}$	0.103(1)	0.113(3)	[28]
$5s$-$5p_{1/2}$	9.49(3)	9.489(10)	[28]	$5s$-$5p_{3/2}$	13.40(4)	13.40(2)	[28]	$3d_{3/2}$-$10p_{3/2}$	0.079(1)		
		9.497	[29]			13.410	[29]	$3d_{5/2}$-$6p_{3/2}$	1.39(1)	1.39(1)	[28]
$5s$-$6p_{1/2}$	0.90(1)	0.91(1)	[28]	$5s$-$6p_{3/2}$	1.30(2)	1.312(6)	[28]	$3d_{5/2}$-$7p_{3/2}$	0.673(7)	0.676(10)	[28]
$5s$-$7p_{1/2}$	0.335	0.341(5)	[28]	$5s$-$7p_{3/2}$	0.491	0.499(5)	[28]	$3d_{5/2}$-$8p_{3/2}$	0.428(4)	0.432(5)	[28]
$5s$-$8p_{1/2}$	0.183(3)			$5s$-$8p_{3/2}$	0.271(4)			$3d_{5/2}$-$9p_{3/2}$	0.308(4)	0.339(5)	[28]
$5s$-$9p_{1/2}$	0.120(2)			$5s$-$9p_{3/2}$	0.178(3)			$3d_{5/2}$-$10p_{3/2}$	0.238(3)		
$5s$-$10p_{1/2}$	0.087(1)			$5s$-$10p_{3/2}$	0.129(2)			$3d_{3/2}$-$4f_{5/2}$	12.3(2)	12.4(1)	[28]
$5p_{1/2}$-$6s$	8.79(2)	8.76(1)	[28]	$5p_{3/2}$-$6s$	12.50(2)	12.47(2)	[28]	$3d_{3/2}$-$5f_{5/2}$	4.92(2)	4.95(3)	[28]
		8.777	[29]			12.490	[29]	$3d_{3/2}$-$6f_{5/2}$	2.899(8)	2.908(30)	[28]
$5p_{1/2}$-$7s$	1.801(8)	1.814(10)	[28]	$5p_{3/2}$-$7s$	2.54(1)	2.56(1)	[28]	$3d_{3/2}$-$7f_{5/2}$	2.001(5)	2.002(20)	[28]
$5p_{1/2}$-$8s$	0.912(5)	0.918(6)	[28]	$5p_{3/2}$-$8s$	1.287(7)	1.310(6)	[28]	$3d_{5/2}$-$4f_{5/2}$	3.27(4)	3.32(3)	[28]
$5p_{1/2}$-$9s$	0.592(3)			$5p_{3/2}$-$9s$	0.834(4)			$3d_{5/2}$-$5f_{5/2}$	1.315(6)	1.322(10)	[28]
$5p_{1/2}$-$10s$	0.430(2)			$5p_{3/2}$-$10s$	0.607(3)			$3d_{5/2}$-$6f_{5/2}$	0.775(2)	0.777(10)	[28]
$5p_{1/2}$-$11s$	0.334(2)			$5p_{3/2}$-$11s$	0.471(3)			$3d_{5/2}$-$7f_{5/2}$	0.535(1)	0.535(10)	[28]
$5p_{1/2}$-$3d_{3/2}$	7.16(10)	7.28(13)	[28]	$5p_{3/2}$-$3d_{3/2}$	3.19(5)	3.24(5)	[28]	$3d_{5/2}$-$4f_{7/2}$	14.6(2)	14.84(12)	[28]
		7.169	[29]			3.193	[29]	$3d_{5/2}$-$5f_{7/2}$	5.88(3)	5.91(4)	[28]
$5p_{1/2}$-$4d_{3/2}$	17.04(6)	16.97(24)	[28]	$5p_{3/2}$-$4d_{3/2}$	7.64(3)	7.61(10)	[28]	$3d_{5/2}$-$6f_{7/2}$	3.47(1)	3.46(3)	[28]
		17.040	[29]			7.643	[29]	$3d_{5/2}$-$7f_{7/2}$	2.392(6)	2.386(20)	[28]
$5p_{1/2}$- $5d_{3/2}$	0.931(35)	1.138(10)	[28]	$5p_{3/2}$-$5d_{3/2}$	0.398(16)	0.490(5)	[28]				
$5p_{1/2}$-$6d_{3/2}$	0.063(14)	0.059(5)	[28]	$5p_{3/2}$-$6d_{3/2}$	0.039(6)	0.015(5)	[28]				
$5p_{1/2}$-$7d_{3/2}$	0.219(11)			$5p_{3/2}$-$7d_{3/2}$	0.105(5)						
$5p_{1/2}$-$8d_{3/2}$	0.236(9)			$5p_{3/2}$-$8d_{3/2}$	0.111(4)						
$5p_{1/2}$-$9d_{3/2}$	0.222(7)			$5p_{3/2}$-$9d_{3/2}$	0.103(3)						

[a]Expt. [31].
[b]Determined from Stark shift data in [14].

in particular contributions for higher excitations, are very large. We have included the estimate of such higher excitation correlations omitted in [28]. We note that the uncertainty evaluation procedure used in [28] [taking the difference of the CCSD and CCSD(T) results] may significantly underestimate the uncertainties since it only works for cases where the perturbative triple contributions are the dominant high-excitation corrections, which is not the case for these transitions. Our results for these transitions are in good agreement with RCICP values [29].
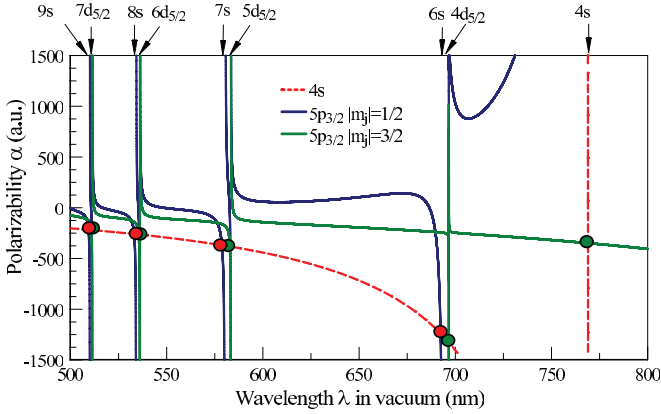
FIG. 1. (Color online) The frequency-dependent polarizabilities of the K $4s$ and $4p_{3/2}$ states. The magic wavelengths are marked with circles. The approximate positions of the $4p_{3/2}$-nl resonances are indicated by vertical lines with small arrows on top of the graph, together with the corresponding nl.

Our results for scalar and tensor polarizabilities of the $4p_j$ excited states of potassium are compared with theoretical [27–30,32] and experimental values [26,33] in Table II. The uncertainty in the experimental measurement [33] of the scalar polarizability is too large to reflect on the accuracy of the present calculations. Extensive comparison of the theoretical and experimental static polarizabilities for the alkali-metal atoms was recently given in the review [40].

III. MAGIC WAVELENGTHS

We define the magic wavelength λ_{magic} as the wavelength for which the ac polarizabilities of two states involved in the atomic transition are the same, leading to a vanishing ac Stark shift of that transition. For the ns-np transitions, a magic wavelength is represented by the point at which two curves, $\alpha_{ns}(\lambda)$ and $\alpha_{np}(\lambda)$, intersect as a function of the wavelength λ. The
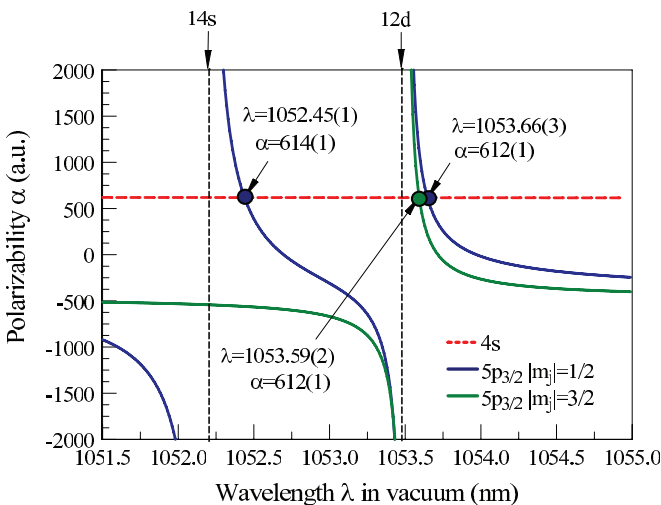
TABLE II. Values of scalar (α_0) and tensor (α_2) polarizabilities in K. The present results are compared with theoretical [27–30,32] and experimental values [26,33]. All values are in atomic units.

	Present	Theory	Expt.
$\alpha_0(4s_{1/2})$	290.4(6)	290.2(8) [32]	290.8(1.4) [26]
		290.5(1.0) [28]	
		289.8(6) [30]	
		290.1 [29]	
$\alpha_0(4p_{1/2})$	612(5)	604.1 [27]	587(87) [33]
		606(7) [28]	
		605.3 [30]	
$\alpha_0(4p_{3/2})$	621(4)	614.1 [27]	613(103) [33]
		614(6) [28]	
		616.0 [30]	
$\alpha_2(4p_{3/2})$	−109.4(1.1)	−107.9 [27]	
		−106(2) [28]	
		−107.5 [30]	
$\alpha_0(3d_{3/2})$	1420(30)	1465.5(21.5) [28]	
$\alpha_0(3d_{5/2})$	1412(30)	1452.8(32.5) [28]	
$\alpha_2(3d_{3/2})$	−482(19)	−502.6(12.5) [28]	
$\alpha_2(3d_{5/2})$	−673(23)	−701.7(25.6) [28]	
$\alpha_0(5s_{1/2})$	4961(22)		
$\alpha_0(5p_{1/2})$	7052(70)		
$\alpha_0(5p_{3/2})$	7230(60)		
$\alpha_2(5p_{3/2})$	−1065(18)		

total polarizability for the $np_{3/2}$ states is given by $\alpha = \alpha_0 - \alpha_2$ for $m_j = \pm 1/2$ and $\alpha = \alpha_0 + \alpha_2$ for the $m_j = \pm 3/2$ case. Therefore, the total polarizability of the $np_{3/2}$ state depends upon its m_j quantum number and the magic wavelengths need to be determined separately for the cases with $m_j = \pm 1/2$ and $m_j = \pm 3/2$ for the ns-$np_{3/2}$ transitions, owing to the presence of the tensor contribution to the total polarizability of the $np_{3/2}$ state. The uncertainties in the values of magic wavelengths are found as the maximum differences between the central value and the crossings of the $\alpha_{ns} \pm \delta\alpha_{ns}$ and $\alpha_{np} \pm \delta\alpha_{np}$ curves, where the $\delta\alpha$ are the uncertainties in the corresponding ns and np polarizability values. All calculations are carried out for linear polarization. Several magic wavelengths were calculated for the $4s$-$4p_{1/2}$ and $4s$-$4p_{3/2}$ transitions in K in Ref. [14] using the all-order approach. Only the magic wavelengths with $\lambda > 600$ nm were listed. In this work, we present several other magic wavelengths for these D_1, D_2 transitions above 500 nm.

The frequency-dependent polarizabilities of the $4s$ and $4p_{3/2}$ states for $\lambda = 500$–800 nm are plotted in Fig. 1. The magic wavelengths are marked with circles. The approximate positions of the $4p_{3/2}$-nl resonances are indicated by vertical lines with small arrows on top of the graph, together with the corresponding nl. For example, the arrow labeled $7s$ indicates the position of the $4p_{3/2}$-$7s$ resonance. The corresponding magic wavelengths are listed in Table III. The results are compared with Ref. [28] where available. We note that the $4p_{3/2}$-$5s$ resonance wavelength is outside of the plot region at $\lambda = 1253$ nm. While there are eight magic wavelengths for the $4s$-$4p_{3/2}|m_j| = 1/2$ transition in the wavelength region shown on the plot, there are only four magic wavelengths for the $4s$-$4p_{3/2}|m_j| = 3/2$ transition since there are no

FIG. 2. (Color online) The frequency-dependent polarizabilities of the K $4s$ and $5p_{3/2}$ states. The magic wavelengths are marked with circles and arrows. The approximate positions of the $5p_{3/2}$-$14s$ and $5p_{3/2}$-$12d$ resonances are indicated by vertical lines with small arrows on top of the graph.

TABLE III. Magic wavelengths for the $4s$-np_j transitions in K. The 500–1227 nm and 1050–1130 wavelength ranges were considered for the $4s$-$4p_j$ and $4s$-$5p_j$ transitions, respectively. The corresponding polarizabilities are given in a.u. The resonances near the magic wavelengths are listed in the first column. The results are compared with Ref. [28].

| Resonances	λ_{magic}	α	Ref.
	$4s$-$4p_{1/2}$ transition		
$4p_{1/2}$-$9s$	508.11(1)	$-214(1)$	
$4p_{1/2}$-$7d_{3/2}$	509.46(1)	$-216(1)$	
$4p_{1/2}$-$8s$	531.79(1)	$-255(1)$	
$4p_{1/2}$-$6d_{3/2}$	533.99(2)	$-259(1)$	
$4p_{1/2}$-$7s$	577.35(2)	$-363(1)$	
$4p_{1/2}$-$5d_{3/2}$	581.04(1)	$-374(1)$	
$4p_{1/2}$-$6s$	690.16(1)	$-1189(2)$	
	690.12(2)	$-1190(3)$	[28]
$4p_{1/2}$-$4s$	768.413(3)	21039(59)	
	768.412(3)	21072(45)	[28]
$4p_{1/2}$-$5s,3d_{3/2}$	1227.67(13)	473(1)	
	1227.2(2)	474(2)	[28]
	$4s$-$4p_{3/2}$, $|m_j| = 1/2$ transition		
$4p_{3/2}$-$9s$	509.36(1)	$-216(1)$	
$4p_{3/2}$-$7d_{5/2}$	511.04(1)	$-218(1)$	
$4p_{3/2}$-$8s$	533.05(1)	$-257(1)$	
$4p_{3/2}$-$6d_{5/2}$	535.72(1)	$-262(1)$	
$4p_{3/2}$-$7s$	578.69(2)	$-367(1)$	
$4p_{3/2}$-$5d_{5/2}$	583.07(1)	$-380(1)$	
$4p_{3/2}$-$6s$	692.33(1)	$-1229(2)$	
	692.26(3)	$-1230(3)$	[28]
$4p_{3/2}$-$4s$	769.432(2)	$-27237(60)$	
	769.43(2)	$-27267(63)$	[28]
$4p_{3/2}$-$5s,3d_j$	1227.65(14)	473(1)	
	1227.8(2)	474(2)	[28]
	$4s - 4p_{3/2}$, $|m_j| = 3/2$ Transition		
$4p_{3/2}$-$7d_{5/2}$	510.74(3)	$-218(1)$	
$4p_{3/2}$-$6d_{5/2}$	535.37(3)	$-261(1)$	
$4p_{3/2}$-$5d_{5/2}$	582.79(2)	$-379(1)$	
$4s - 4p_j$	768.980(2)	$-348(3)$	
	768.98(2)	$-336.52(6)$	[28]
	$4s$-$5p_{1/2}$ transition		
$5p_{1/2}$-$14s$	1050.24(1)	617(1)	
$5p_{1/2}$-$12d_{3/2}$	1051.53(3)	615(1)	
$5p_{1/2}$-$13s$	1067.33(1)	595(1)	
$5p_{1/2}$-$11d_{3/2}$	1069.02(3)	593(1)	
$5p_{1/2}$-$12s$	1090.79(1)	570(1)	
$5p_{1/2}$-$10d_{3/2}$	1093.06(5)	567(1)	
$5p_{1/2}$-$11s$	1124.42(1)	539(1)	
$5p_{1/2}$-$9d_{3/2}$	1127.56(2)	536(1)	
	$4s$-$5p_{3/2}$, $|m_j| = 1/2$ transition		
$5p_{3/2}$-$14s$	1052.45(1)	614(1)	
$5p_{3/2}$-$12d_{3/2}$	1053.66(3)	612(1)	
$5p_{3/2}$-$13s$	1069.67(1)	593(1)	
$5p_{3/2}$-$11d_{3/2}$	1071.23(4)	591(1)	
$5p_{3/2}$-$12s$	1093.32(2)	567(1)	
$5p_{3/2}$-$10d_{3/2}$	1095.40(6)	565(1)	
$5p_{3/2}$-$11s$	1127.29(2)	536(1)	
$5p_{3/2}$-$9d_{3/2}$	1130.10(2)	534(1)	
	$4s$-$5p_{3/2}$, $|m_j| = 3/2$ transition		
$5p_{3/2}$-$12d_{3/2}$	1053.59(2)	612(1)	
$5p_{3/2}$-$11d_{3/2}$	1071.15(3)	591(1)	
$5p_{3/2}$-$10d_{3/2}$	1095.28(4)	565(1)	
$5p_{3/2}$-$9d_{3/2}$	1129.91(1)	534(1)	
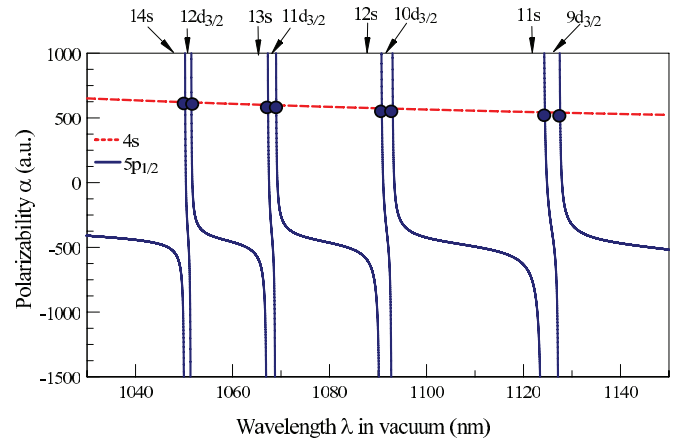
FIG. 3. (Color online) The frequency-dependent polarizabilities of the K $4s$ and $5p_{1/2}$ states. The magic wavelengths are marked with circles. The approximate positions of the $5p_{1/2}$-nl resonances are indicated by vertical lines with small arrows on top of the graph, together with the corresponding nl.

corresponding crossings near the $4p_{3/2}$-ns resonances as in the case of $|m_j| = 1/2$. The 769 nm magic wavelength for the $|m_j| = 1/2$ is not shown on the plot since the corresponding polarizability (-27237 a.u.) is outside of the plot y-axis range. There is only one magic wavelength above 800 nm for the $4s$-$4p_{3/2}|m_j| = 1/2$ transition due to $4p_{3/2}$-$5s$ resonance and none for the $|m_j| = 3/2$ case. The magic wavelengths for the $4s$-$4p_{1/2}$ transition are very close to those for $4s$-$4p_{3/2}|m_j| = 1/2$. They are also given in Table III.

The magic wavelengths for the UV $4s$-$5p_j$ transitions are completely different than those for the D_1, D_2 lines owing to completely different sets of resonances. The K case is also significantly different from that of Li [36] due to differences in the resonant transition wavelengths. We list the magic wavelengths for the $4s$-$5p_{1/2}$ and $4s$-$5p_{3/2}$ transitions in the range of 1050–1130 nm, which is of particular experimental
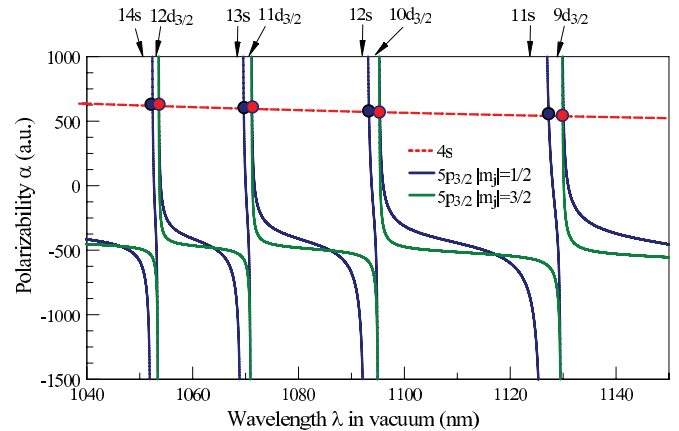
FIG. 4. (Color online) The frequency-dependent polarizabilities of the K $4s$ and $5p_{3/2}$ states. The magic wavelengths are marked with circles. The approximate positions of the $5p_{3/2}$-nl resonances are indicated by vertical lines with small arrows on top of the graph, together with the corresponding nl.

interest in Table III. We find 20 magic wavelengths in the technical interest region of 1050–1130 nm accessible by a number of widely used lasers. The magic wavelengths for the $4s$-$5p_{3/2}$ transition near 1053 nm wavelength are illustrated in Fig. 2. As in the case of the $4s$-$4p_{3/2}$ transition, there is no magic wavelength for the $|m_j| = 1/2$ case near the ns resonance. All magic wavelengths for the $4s$-$5p_{1/2}$ and $4s$-$5p_{3/2}$ transitions in the range of 1050–1140 nm are illustrated in Figs. 3 and 4. The same designations are used as in the previous graphs. Comparing these figures with the similar plots for Li (see Figs. 3 and 4 of Ref. [36]) shows that K magic wavelengths near 1050–1130 nm originate from crossings near much higher resonances ($n = 9$–14 vs $n = 6$–7 for Li) making the calculation for K more complicated due to the very large cavity size required to accommodate such highly excited orbitals.

IV. CONCLUSION

We have calculated the ground $4s$, $4p$, and $5p$ state ac polarizabilities in K using the relativistic linearized coupled-cluster method and evaluated the uncertainties of these values. We have used our calculations to identify the magic wavelengths for the $4s$-$4p$ and $4s$-$5p$ transitions. The magic wavelengths for the ultraviolet resonance lines are of particular interest for laser cooling of ultracold gases with high phase-space densities.

[1] L. Yi, S. Mejri, J. J. McFerran, Y. LeCoq, and S. Bize, Phys. Rev. Lett. **106**, 073005 (2011).

[2] D. C. McKay, D. Jervis, D. J. Fine, J. W. Simpson-Porco, G. J. A. Edge, and J. H. Thywissen, Phys. Rev. A **84**, 063420 (2011).

[3] N. Lundblad, M. Schlosser, and J. V. Porto, Phys. Rev. A **81**, 031611(R) (2010).

[4] A. D. Ludlow, T. Zelevinsky, G. K. Campbell, S. Blatt, M. M. Boyd, M. H. G. de Miranda, M. J. Martin, J. W. Thomsen, S. M. Foreman, J. Ye *et al.*, Science **319**, 1805 (2008).

[5] A. Derevianko, Phys. Rev. Lett. **105**, 033002 (2010).

[6] H. Katori, K. Hashiguchi, E. Y. Il'inova, and V. D. Ovsiannikov, Phys. Rev. Lett. **103**, 153004 (2009).

[7] V. A. Dzuba, V. V. Flambaum, and B. L. Lev, Phys. Rev. A **83**, 032502 (2011).

[8] S. Zhang, F. Robicheaux, and M. Saffman, Phys. Rev. A **84**, 043408 (2011).

[9] U. Dammalapati, B. Santra, and L. Willmann, J. Phys. B **45**, 025001 (2012).

[10] Y. Geng-Hua, Z. Jia-Qi, L. Run-Bing, W. Jin, and Z. Ming-Sheng, Chin. Phys. Lett. **28**, 073201 (2011).

[11] M. S. Safronova, D. Jiang, M. G. Kozlov, and U. I. Safronova, in *IEEE International Conference on Frequency Control Symposium (FCS), 1–4 June 2010* (IEEE, Piscataway, NJ, 2010), pp. 59–64.

[12] A. Ye and G. Wang, Phys. Rev. A **78**, 014502 (2008).

[13] K. Guo, G. Wang, and A. Ye, J. Phys. B **43**, 135004 (2010).

[14] B. Arora, M. S. Safronova, and C. W. Clark, Phys. Rev. A **76**, 052509 (2007).

[15] Z. Yu-Nan, Z. Xiao-Ji, C. Jing-Biao, and C. Xu-Zong, Chin. Phys. Lett. **23**, 1687 (2006).

[16] H. Katori, T. Ido, and M. Kuwata-Gonokami, J. Phys. Soc. Jpn. **668**, 2479 (1999).

[17] J. Ye, D. W. Vernooy, and H. J. Kimble, Phys. Rev. Lett. **83**, 4987 (1999).

[18] P. M. Duarte, R. A. Hart, J. M. Hitchcock, T. A. Corcovilos, T.-L. Yang, A. Reed, and R. G. Hulet, Phys. Rev. A **84**, 061406(R) (2011).

[19] J. McKeever, J. R. Buck, A. D. Boozer, A. Kuzmich, H.-C. Nägerl, D. M. Stamper-Kurn, and H. J. Kimble, Phys. Rev. Lett. **90**, 133602 (2003).

[20] M. S. Safronova, C. J. Williams, and C. W. Clark, Phys. Rev. A **67**, 040303 (2003).

[21] M. Saffman and T. G. Walker, Phys. Rev. A **72**, 022347 (2005).

[22] B. Arora, M. S. Safronova, and C. W. Clark, Phys. Rev. A **82**, 022509 (2010).

[23] L. J. LeBlanc and J. H. Thywissen, Phys. Rev. A **75**, 053612 (2007).

[24] B. Arora, M. S. Safronova, and C. W. Clark, Phys. Rev. A **84**, 043401 (2011).

[25] W. F. Holmgren, R. Trubko, I. Hromada, and A. D. Cronin, Phys. Rev. Lett. **109**, 243004 (2012).

[26] W. F. Holmgren, M. C. Revelle, V. P. A. Lonij, and A. D. Cronin, Phys. Rev. A **81**, 053607 (2010).

[27] U. I. Safronova and M. S. Safronova, Phys. Rev. A **78**, 052504 (2008).

[28] D. K. Nandy, Y. Singh, B. P. Shah, and B. K. Sahoo, Phys. Rev. A **86**, 052517 (2012).

[29] J. Jiang, L.-Y. Tang, and J. Mitroy, Phys. Rev. A **87**, 032518 (2013).

[30] B. K. Sahoo and B. Arora, Phys. Rev. A **87**, 023402 (2013).

[31] S. Falke, I. Sherstov, E. Tiemann, and C. Lisdat, J. Chem. Phys. **125**, 224303 (2006).

[32] A. Derevianko, W. R. Johnson, M. S. Safronova, and J. F. Babb, Phys. Rev. Lett. **82**, 3589 (1999).

[33] R. Marrus and J. Yellin, Phys. Rev. **177**, 127 (1969).

[34] W. R. Johnson, U. I. Safronova, A. Derevianko, and M. S. Safronova, Phys. Rev. A **77**, 022510 (2008).

[35] M. S. Safronova and U. I. Safronova, Phys. Rev. A **83**, 052508 (2011).

[36] M. S. Safronova, U. I. Safronova, and C. W. Clark, Phys. Rev. A **86**, 042505 (2012).

[37] M. S. Safronova and W. R. Johnson, Adv. At. Mol. Opt. Phys. **55**, 191 (2008).

[38] J. Mitroy and M. S. Safronova, Phys. Rev. A **79**, 012513 (2009).

[39] M. S. Safronova, S. G. Porsev, M. G. Kozlov, and C. W. Clark, Phys. Rev. A **85**, 052506 (2012).

[40] J. Mitroy, M. S. Safronova, and C. W. Clark, J. Phys. B **43**, 202001 (2010).

[41] Yu. Ralchenko, A. Kramida, J. Reader, and NIST ASD Team, NIST Atomic Spectra Database (version 4.1) [http://physics.nist.gov/asd], National Institute of Standards and Technology, Gaithersburg, MD (2011).